Commun Nonlinear Sci Numer Simulat 82 (2020) 105024

Contents lists available at ScienceDirect

Commun Nonlinear Sci Numer Simulat

journal homepage: www.elsevier.com/locate/cnsns

Research paper

Concomitance of inverse stochastic resonance and stochastic resonance in a minimal bistable spiking neural circuit

AmirPasha Zamani [a], Nikita Novikov [b], Boris Gutkin [a,b,*]

[a] Centre for Cognition and Decision Making, National Research University Higher School of Economics, Moscow 101000, Russia
[b] Group for Neural Theory and LNC2 INSERM U960, Department of Cognitive Studies, Ecole Normale Superieure PSL* Research University, Paris 75005, France

ARTICLE INFO

Article history:
Available online 25 September 2019

Keywords:
Persistent activity
Stochastic resonance
Inverse stochastic resonance
Mutual Information

ABSTRACT

Stochastic Resonance (SR) is a well-known noise-induced phenomenon widely reported in dynamical systems with a threshold, while Inverse Stochastic Resonance (ISR) is an opposing phenomenon observed in the dynamical systems which exhibit bistability between a stable node and a stable limit cycle. This study shows a co-occurrence of SR and ISR, in a minimal circuit of synaptically coupled spiking neurons that is designed to show bistability between quiescence and a persistent firing mode. We identify noise, synaptic and intrinsic parameters ranges that allow for ISR. The minimal computational model, is investigated for a range of parameters, and our simulations indicate that the main features of SR, are the direct results of dynamical properties which lead to ISR.

1. Introduction

Self-sustained neural activities have been reported in various brain areas including the Prefrontal [1,2], and entorhinal cortex [3–5] medial temporal lobe [6], parahipocampal and [7,8] several subcortical regions such as basal ganglia [9], thalamus [10], superior colliculus [11], brain stem [12], and spinal cord [13]. Therefore, these activities are suggested to have a universal form of circuit dynamics, responsible for accumulation of sensory or motor information, executive control, attentional modulation, and more importantly for short-term information storage during working memory [14]. In addition, the active memory retention in such neural circuits by self-sustained firing – or so called 'persistent activity' – is robust to noise and irrelevant distractor stimuli [1,4]. The widely accepted hypothesis as to the underlying mechanisms of persistent activities in the brain, relies on synaptic reverberations in recurrent circuits with appropriate levels of interconnectivity [15,16].

Considering the effect of noise when modeling neural systems is important since random perturbations are ubiquitous at many different scales, ranging from molecular to large brain networks, either intrinsic to the cells and ion channels or coming from external sources [17]. Diverse influence on neural activities, both promoting [18] and inhibiting (e.g. [19]), have been identified for noise in the neural systems. It has even been proposed that the nervous system has evolved not only to adapt to the unavoidable random perturbations, but also to use the functional advantage of noise [17]. One such situation is

* Corresponding author at: Group for Neural Theory and LNC2 INSERM U960, Department of Cognitive Studies, Ecole Normale Superieure PSL* Research University, Paris 75005, France.
E-mail address: boris.gutkin@ens.fr (B. Gutkin).

https://doi.org/10.1016/j.cnsns.2019.105024

when specific levels of noise can promote neural activity to transmit an otherwise sub-threshold signal inducing stochastic resonance [24–26].

1.1. Stochastic resonance

There is an extensive literature on Stochastic Resonance whose comprehensive review is beyond the scope of this paper. A seminal review by Wiesenfelt and Moss [20], pointed out that, although engineers had always sought to minimize the effect of noise in electrical and communicational circuits, noise can play a constructive role in detection of weak periodic signals, via a mechanism so called Stochastic Resonance (SR). The primary signature of SR, which had been observed in a variety of settings, such as meteorological [21], and electrical [22,23] systems, as well as in a biological organism (e.g. in crayfish mechanoreceptors) [24], was the improvement of information transfer, by the presence of a particular optimal non-zero level of noise. Later SR was reported in further biological organisms, such as paddlefish [25] and in computational models of neurons [26,27]. In neuroscience SR appears to be a phenomenon present at multiple levels of neural organization. Landmark experiments in psychophysics, electrophysiology, animal behavior, fMRI, human vision, hearing and tactile function, plus single and multiunit activity recordings all have shown SR (reviewed in [28]).

For the framework considered in this report, SR can be defined as a phenomenon in which the time scale imposed by an external signal becomes commensurate with an appropriate switching rate of a bistable dynamical system between its two stable states [27]. The effects can be quantitatively characterized using signal transfer measures, such as signal-to-noise ratios and/or information theoretic measures. As such, the noise-induced switching phenomenon, would make the amount of information transfer, and thus the Mutual Information (MI) between the input signal and output of a bistable system, to be maximal at a specific intermediate level of noise [29,30].

1.2. Inverse stochastic resonance

About two decades after the discovery of SR, a novel effect of tuned noise on nonlinear dynamical systems emerged [31], suggesting that, noise, hitherto assumed to advance bifurcations in multi-stable systems, delays switching in bistable neural oscillators. In that work, the minimal network comprised of two synaptically connected theta neurons which excited each other reciprocally and produced sustained firing. Notably, the theta-neurons were mono-stable (excitable), hence the sustained activity was due to the reciprocal excitation. Also notably, firing in the synaptically sustained state was anti-synchronous and unstable to forced synchronization. The observed effect of zero-mean noise there was cessation or diminution of firing activity at a tuned level of noise, forming a U-shaped function of firing rate versus the noise intensity [31]. This was termed Inverse Stochastic Resonance [35]. Such non-intuitive effect of noise on the dynamics of the neural activity, was shown not only restricted to coupled neurons, but generalizable to bistable dynamical systems with a stable limit cycle and a stable fixed point coexisting [32]. It was different from the kind of bistability discussed in the previous works on SR, which was bistability between two stable fixed points.

In follow up studies [33,34] termination of activity was portrayed in terms of probability of escape from the attraction domain of the periodic attractor and absorption by the stable rest point. This phenomenon replicated in single Hodgkin-Huxley neuronal models [19,35,36,37] and was also observed in experimental studies in squid axon firing and activity of cerebellar Purkinje cells [38,39]. Moreover, it was suggested that although ISR diminishes persistent activity, it is not necessarily a negative impact, but it might be a mechanism for enriching the intrinsic stochastic dynamics of biological neural systems [40].

In general, there are three key features seen as the underlying dynamical structure of a nonlinear system which manifests ISR: (1) The coexistence of a limit cycle and a stable resting equilibrium. (2) The relative proximity of the basin boundary to the stable limit cycle so that a small noise would easily deviate the phase trajectories from the limit cycle and force them to the attraction domain of the rest. (3) And the relatively far distance of the boundary from the rest point for large majority of the limit cycle orbit [37].

1.3. SR and ISR in the same system

We hypothesize that a dynamical system which exhibits ISR due to noise-induced transitions from its periodically active mode to its silent mode, is disposed to SR also, provided it receives an external synaptic input to represent its temporal structure in the firing pattern of the output. In the present paper we investigate this hypothesis numerically, exploiting a minimal network of two-neurons, that are coupled to synaptically excite each other reciprocally and to produce persistent patterns of firing, resembling minimal models of working memory [16].

To investigate the potential co-occurrence of ISR and SR, we introduce the minimal spiking neuronal model and briefly characterize its dynamics, mapping out the activity regions of the system and the bifurcation borders separating the bistable, silent-mono-stable, and oscillatory-mono-stable modes of activity. Then, a random wiener process will be injected to the system to study the effect of noise on the course of persistent firing. The noise induced properties in the network, will be investigated at 12 exemplary parameter points, with different distances from the borders of bifurcation.

Next, to study the SR effect in the circuit, we will extend the two-neuron network by introducing a third neuron, providing a periodic synaptic input to the neurons in the recurrently coupled pair. We will compute the Mutual Information

as a measure to quantify the amount of information transfer from the stimulus to the network. In this condition the stimulus effect, on the firing pattern of the original network will be investigated at the very same parameter points where ISR was studied. It will be shown that the U-shaped ISR curves are correlated with the bell-shaped SR curves. Lastly, we map out the attraction domains of the attractive states in the phase plane to identify the dynamical features, which lead to the co-occurrence of SR and ISR.

2. Model set up and methods

To investigate different noise-induced effects in a minimal network of neurons, we have employed the Quadratic Integrate and Fire (QIF), a nonlinear and simple point neuron model, whose spike generating mechanism complies with the behavior of type 1 cortical cells [41].

2.1. Coupling two neurons

For the basic network, two intercoupled individual QIF neurons with a resetting mechanism are given by the following system of equations:

$$\begin{aligned} \frac{dX}{dt} &= X^2 + I_{ext} + I_{syn}^X \\ if\ X &= V_{peak} \ \rightarrow \ X = V_{reset} \\ \frac{dY}{dt} &= Y^2 + I_{ext} + I_{syn}^Y \\ if\ Y &= V_{peak} \ \rightarrow \ Y = V_{reset} \end{aligned} \tag{1}$$

X and Y are the membrane potentials of the first and the second neuron, each one varying in the range $[V_{reset}\,.V_{peak}]$ such that whenever each membrane potential exceeds $V_{peak} = 80\ mv.$ it resets back to the reset point $V_{reset} = -8\ mv$. This reset is set to mimic cortical pyramidal neurons, and since its value is always smaller than the resting membrane potential, $V_{rest} = -\sqrt{|I_{ext}|}$, it leads to an undershoot in the cell voltage, followed by an exponential increase toward the rest state. The model parameters are chosen close to the Hodgkin Huxley model of [32].

I_{ext} is a constant parameter determining the excitability mode and, stable states of the individual cells. In general, when I_{ext} is below zero, each neuron is excitable with a stable node (rest) and a repeller (threshold). I_{syn} for each neuron, is the recurrent input provided by the other cell through an exponential time dependent synapse with the following system of equations:

$$\begin{aligned} I_{syn}^x &= J \cdot e^{-\left(\frac{t-t_y}{\tau_s}\right)} \cdot U(t-t_y) \\ I_{syn}^y &= J \cdot e^{-\left(\frac{t-t_x}{\tau_s}\right)} \cdot U(t-t_x) \end{aligned} \tag{2}$$

here t_x and t_y are the time points at which neurons X and Y hit their peak voltage values respectively; and the function $U(t-t_i)$ is a standard step function, allowing the synaptic current to initiate at time t_i, $i \in \{x.y\}$. Consequently, as soon as X (Y) produces an action potential, it provides an abrupt synaptic current of size J, as an input to Y (X). This synaptic current decays exponentially with a synaptic time constant, $\tau_s = 5\ ms$, which is always shorter than the period of sustained activities, in our settings.

While neurons are uncoupled ($I_{syn} = 0$) and $I_{ext} < 0$, each individual cell has two equilibria, $x.y = \pm\sqrt{|I_{ext}|}$. The negative value that is a stable fixed point for the model, plays the role of the rest state in biological neurons, and the positive value, which is an unstable fixed point, represents the threshold for spike generation. In such a condition, the neuron is said to be at a mono-stable-excitable mode of activity; that means a stable rest point coexist with infinite amplitude heteroclinic solutions (formally speaking linking the repeller to the rest point through a blow up to infinity and a reentry from negative infinity in finite time), which leads to production of a single action potential only when the neuron is shortly triggered externally.

While still uncoupled, and $I_{ext} = 0$, a saddle node bifurcation occurs for the single QIFs, and as a result, for $I_{ext} > 0$ the neuron will be in an oscillatory mono-stable state, periodically firing with no need to any external input.

As it had been shown in [33], mutual coupling of QIF neurons can form a bistable system consisting of a stable rest and a Stable Limit Cycle (SLC). Coexistence of these two stable modes predisposes the occurrence of ISR. In such a system, although the neural components are at their individual excitable region of activity, the network can exhibit an antiphase oscillatory behavior due to the recurrent excitations; or it can be silent when both components are at rest. A sufficiently large synaptic strength is required to cause a global bifurcation resulting in such bistability. In addition to the synaptic strength, J, the global bifurcation point depends also on the value of the external current, I_{ext}. Indeed, the more negative the external current is, the stronger coupling for the occurrence of bifurcation is required. This is illustrated in Fig. 1(b) where different regions of activity are shown in the parameter space J-I_{ext}. Firing rate of the persistent activity at each point is color coded in this figure. The region of interest for the purpose of studying SR and ISR phenomena is the bistable area, close to the global bifurcation border, where random noise can shift the system back and forth between the silent and active modes.

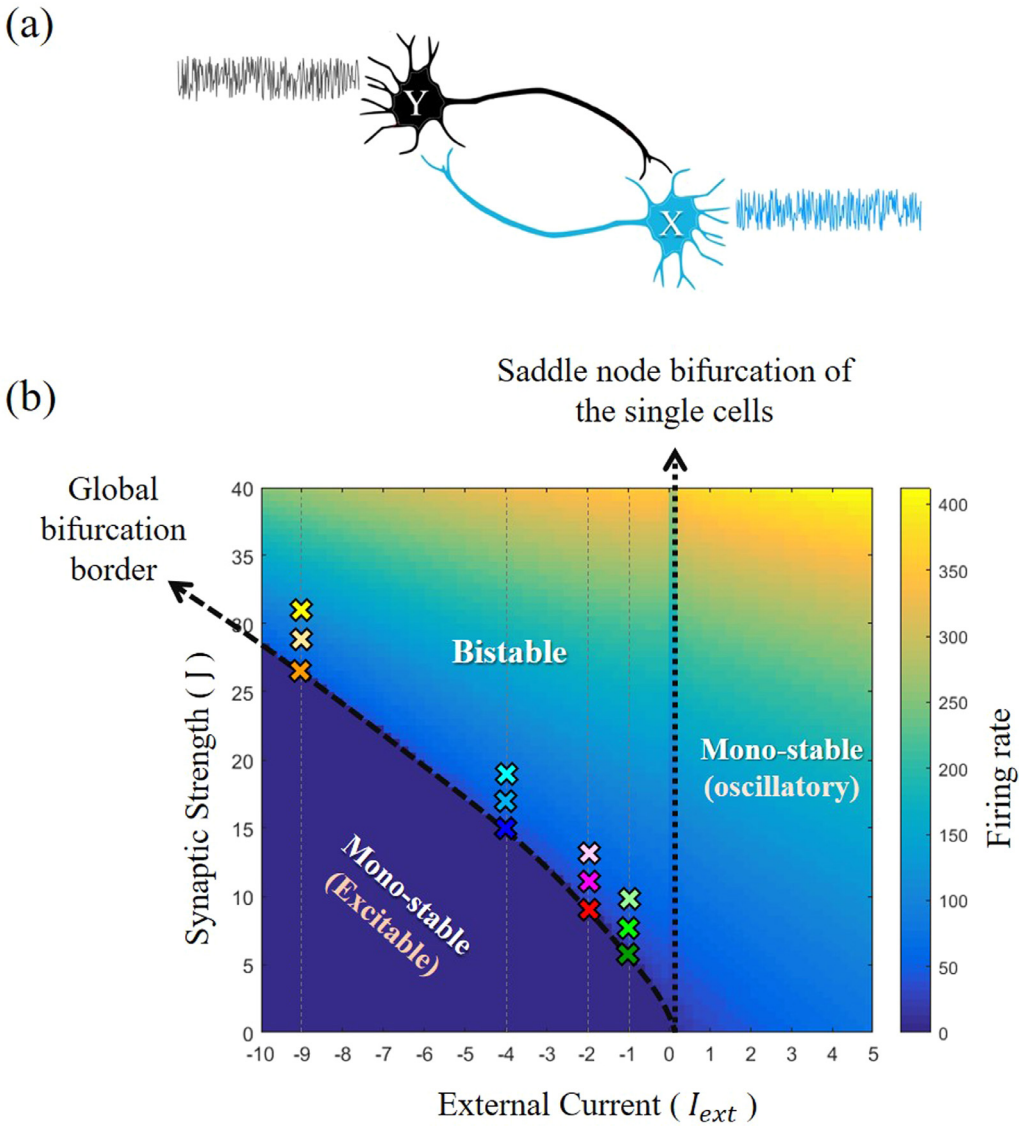

Fig. 1. Schematic and State diagram of the circuit. (a): Neurons X and Y are connected to each other reciprocally and each one receives and independent white noise. (bb): Coupled QIF neurons can work at three different activity regions, depending on the coupling strength, J, and the value of external current, I_ext. When I_extis positive each individual neuron, and thus the whole network is at a mono-stable-oscillatory mode. The vertical line I_ext = 0 is the saddle node bifurcation for the single cells such that to the left of this line, each individual cell is excitable. However, by growing the coupling strength, J, this area is divided into two regions where the network is either excitable or bistable. These three regions of activity are separated with black dashed lines in the parameter space, J- I_ext. The corresponding firing rates at each point are color coded. The 12 colored crosses illustrate the location of selected pairs of parameters which we are going to study the network's features at those points. The numerical values of J and I_ext at these points are given in Table 1. (For interpretation of the references to color in this figure legend, the reader is referred to the web version of this article.)

For illustration purposes, we chose four points to be on the border of the network bifurcation, with firing rates between 20 and 40 Hz. Then, eight other points farther above this border (increasing the synaptic strength from the 4 border points), were selected to be used in simulations and to be compared with each other. All of these points' locations in the parameter space, are marked in Fig. 1, with colored crosses, and their numeric values are given in Table 1. (The criteria for selection of characteristic parameter points is explained in the Supplementary Materials, Section 1.s)

2.2. Inverse stochastic resonance settings

Two random wiener processes with amplitude σ are injected to the network, converting Eq. (1) to the following form:

$$dX = \left(X^2 + I_{ext} + I_{syn}^X\right)dt + \sigma\, dW$$
$$if\ X = V_{peak} \ \rightarrow\ X = V_{reset}$$

Table 1
Selected parameter points for the simulations and the corresponding endogenous Firing Rates (FR).

mark	J	I_{ext}	$FR_{X,Y}$ (Hz)	J_z	I_{ext_Z}	FR_z (Hz)
✖	6	-1	20	5.5	0.1	10
✖	9.3	-2	25	8	0.2	14
✖	14.8	-4	30	14	0.3	17
✖	26.5	-9	40	25	0.3	17
✖	8	-1	42	5.5	0.1	10
✖	11	-2	45	8	0.2	14
✖	17	-4	58	14	0.3	17
✖	29	-9	87	25	0.3	17
✖	10	-1	55	5.5	0.1	10
✖	13	-2	60	8	0.2	14
✖	19	-4	76	14	0.3	17
✖	31	-9	118	25	0.3	17

$$\begin{aligned} dY &= (Y^2 + I_{ext} + I_{syn}^Y)dt + \sigma dW \\ if\ Y &= V_{peak} \quad \rightarrow \quad Y = V_{reset} \end{aligned} \tag{3}$$

To indicate ISR and to identify the noise which can optimally terminate firing, firstly, for switching on the persistent activity, the initial conditions $X(0) = \sqrt{|I_{ext}|} + 0.01$ and $Y(0) = V_{reset}$ are considered in all of the simulations.

Next, the network is left noise-free for 200 ms, to make sure that the transient state has passed and the system is on the SLC. Then, two independent random signals of white noise are separately injected to neurons X and Y for an additional 800 ms. The Mean Firing Rate (MFR) will be acquired over this 800 ms period after the noise onset, and averaged over 1000 trials for a set of different noise levels. The noise amplitude is a free parameter that starts from zero, and increases up to 5, with a step size of 0.1. The circuit schematic diagram is shown in Fig. 1(a).

2.3. Stochastic resonance settings

To quantify the ability of the constructed bistable system to process a time structured input, under noise conditions, a third neuron Z, independent of X and Y, is designed to provide external periodic input to the network:

$$\begin{aligned} dX &= (X^2 + I_{ext} + I_{syn}^X + I_{in}^X)\ dt + \sigma dW \\ if\ X &= V_{peak} \ \rightarrow \ X = V_{reset} \\ dY &= \left(Y^2 + I_{ext} + I_{syn}^Y + I_{in}^Y\right)dt + \sigma dW \\ if\ Y &= V_{peak} \quad \rightarrow \quad Y = V_{reset} \\ \frac{dZ}{dt} &= Z^2 + I_{ext_Z} \\ if\ Z &= V_{peak} \ \rightarrow \ Z = V_{reset} \end{aligned} \tag{4}$$

The third neuron, Z, is a QIF neuron similar to the other two, except that it must have a positive external current (I_{ext_Z}) to fire independently at its oscillatory state, so that it can always provide a periodic synaptic input to the network. Whenever a spike is produced by Z it sends out an exponentially decaying current, I_{syn}^Z, with the very same mechanism as X and Y did:

$$I_{syn}^Z = J_z \cdot e^{-\left(\frac{t-t_z}{\tau_s}\right)} \cdot U(t - t_z) \tag{5}$$

We note that, when the network is uncoupled, the third neuron Z is potentially capable of exciting X and Y and evoke spikes in them, which is not what we want for this study. Thus, the synaptic strength, J_z, is chosen weak enough, such that it cannot excite the network and cause unwanted spikes. On the other hand, it should be large enough, such that a reasonable amount of noise can amplify the input, and make it discernible for the network. The selected J_z values for this purpose are indicated in Table 1.

Different values of I_{ext_Z}, chosen from the set {0.02, 0.05, 0.1, 0.2, 0.3, 0.5, 1} were employed for evaluating the network's reaction to the inputs of various frequencies. These external currents, cause Z, to respectively fire monotonically with the frequencies: {4.5, 7, 10, 14, 17, 23, 27} Hz. At each parameter condition, the appropriate input which is well represented by

the original network is selected for illustration of the SR effect. These selected values and the corresponding firing rates are also indicated in Table 1.

Moreover, in Eq. (4), the extra term, I_{in}, which is added to the inputs of X and Y, is the time structured input that the network is receiving from Z. In this context, X and Y are supposed to represent the input in their patterns of firing. Two different conditions are considered for studying the network's reaction to the external stimulus. In the first setting, a synaptic current produced by Z, arrives simultaneously to both neurons X and Y, i.e. $I_{in}^X = I_{in}^Y = I_{syn}^Z$; while in the second setting, only one of the comprising neurons (X) receives the input, i.e. $I_{in}^Y = 0$ and $I_{in}^X = I_{syn}^Z$.

2.4. Mutual information

The Synapse J_z is treated as a communication channel, conveying the train of presynaptic spikes to the original network, and affecting the spike trains at the post synaptic neurons, *X* and *Y*. To quantify the amount of such effect, or in other words, to specify how much information is transmitted from *Z* to *X* and *Y*, the MI-toolbox of Matlab [42], is employed, to compute the Mutual Information (MI) between the input signal and the output spikes of the network at different noisy conditions. MI, an information theory measure [43,44] is defined by the equation:

$$\mathrm{MI} = \mathrm{H}(\mathrm{S_{out}}) - \mathrm{H}(\mathrm{S_{out}}|\mathrm{S_{in}}) \tag{6}$$

where $H(S_{out})$ is the estimated entropy of the output signal, and $H(S_{out}|S_{in})$ is the conditional entropy of the output, S_{out}, given the input S_{in}.

The entropy denoted *H(S)* itself, is a measure that quantifies the uncertainty present in the distribution of signal *S*, and is defined as:

$$H(S) = -\sum_{s\in\delta} P(s)\ logP(s) \tag{7}$$

here, the lower case *s* denotes a possible value that the random variable *S* can adopt from the alphabet δ, and *P(s)* is the probability distribution function which can be estimated as the fraction of observations taking on value *s* from the total *N* samples; $\hat{P}(s) = \frac{\#s}{N}$. More details on the entropy, conditional entropy, and MI calculations can be found in [45].

In the current context, S_{out} is spiking of either *X* or *Y*, and S_{in} is spiking of *Z*. However, before computing MI, all *X* and *Y* signals must be transformed into binary strings (ones for spike moments and zeros otherwise). In all of the following simulations, the bin-size for the process of discretization, is $\Delta t = 2\ ms$, for the cases where $I_{ext} = -9$, and $\Delta t = 3\ ms$ otherwise. (The criteria for the selection of bin-sizes are given in the Supplementary Materials, Section 2.s)

Then, the mi-toolbox is used for calculation of entropies, conditional entropies, and mutual information between the binary versions of *X* (or *Y*) and *Z* activity. MI is measured during 4 s of simulation and is averaged over 2000 trials. To obtain the SR curves, this average (MI_{mean}) will be plotted versus the noise levels. To visualize the phase space of this system, we convert the membrane potentials into dynamics of a phase variable. Here, we start with the θ-neuron where a neuron is described by a phase variable, θ, indicating the membrane potential's location, along the trajectory of action potentials in the phase space. By a simple substitution $X = \tan\frac{\theta_x}{2}$ and $Y = \tan\frac{\theta_y}{2}$, QIFs can be rewritten as equivalent θ-neurons. The $\theta_x\theta_y$ plane will be exploited for illustrating the time evolution of the phase variables. The phase portrait is 2π periodic on this plane, where the right and the upper sides represent the phase switching from V_{peak} to V_{reset}. The relevant fixed points are also reflected on the phase plane by converting them from the *X,Y* to $\theta_x\theta_y$ coordinates. In summary to visualize the phase plane of the system, with the appropriate parameter conversions, we will plot the variables $\theta_x = 2\mathrm{atan}(X)$, and $\theta_y = 2\mathrm{atan}(Y)$ which are always in an interval between $-\pi$ and π.

3. Results

3.1. Phase plane structure of the minimal circuit

First of all, to explore the general dynamical features of the uncoupled noise-free system, (Eqs. (1) and (2) with $J = 0$) the network phase portrait is plotted in the left panel of Fig. 2(a), illustrating the course of phase trajectories when starting at different arbitrary initial states. The external current for obtaining this figure is set to $I_{ext} = -1$. Initial states are illustrated with small gray squares. The green circle indicates the stable fixed point, where both neurons are at rest. The dashed lines indicate the separatrices of the unstable points, which are in fact the thresholds for spiking. Thus, as it is observed, whenever the initial state of each neuron is beyond these separatrices, the phase trajectory escapes the unstable point, emits a spike by hitting the upper (for Y) or right (for X) side of the plane, enters the plane from the other side (reset), and moves directly to the rest state. The corresponding single spikes, which are emitted in this excitable mode, are shown in the time domain, on the right panel.

As indicated with numbers on the left and right panels of Fig. 2(a), the upper and the right side of the phase plane, are the spike-times for Y and X, respectively, because $\theta = 2\mathrm{atan}(X_{peak}) = 2\mathrm{atan}(80) \approx \pi$. Moreover, due to the periodic nature of the phase-plane, after hitting the voltage peak, phase trajectories continue their paths from the opposite side of the plane at the bottom or left side, where the phase variable is $\theta = 2\mathrm{atan}(X_{reset}) = 2\mathrm{atan}(-8) \approx -2.9$.

Next, the phase portrait of the coupled network (Eqs. (1) and (2)) with synaptic strength $J = 6$, is plotted in the left panel of Fig. 2(b). In this setting, whenever a neuron is reset, the stable rest will attract and hold its phase trajectory, unless the synaptic current by the other neuron, is strong enough to force the membrane potential across the distance between the stable and saddle node, and cause another spike emission. For this to happen, the synaptic coupling, J, must be strong enough, and the neurons must work in an almost antiphase mode, so that they can excite each other reciprocally; otherwise the firing activity will not continue.

In the right panel of Fig. 2(b), in addition to the spike patterns, the signals of synaptic currents which are produced by each cell, and are transferred to the other cell through the coupling, are also shown. We can see that in this condition, the phase trajectories which have started below the threshold borders (gray lines), show no change compared to the previous uncoupled case. However, the other trajectories do not approach the rest state directly after the spike emissions. Instead,

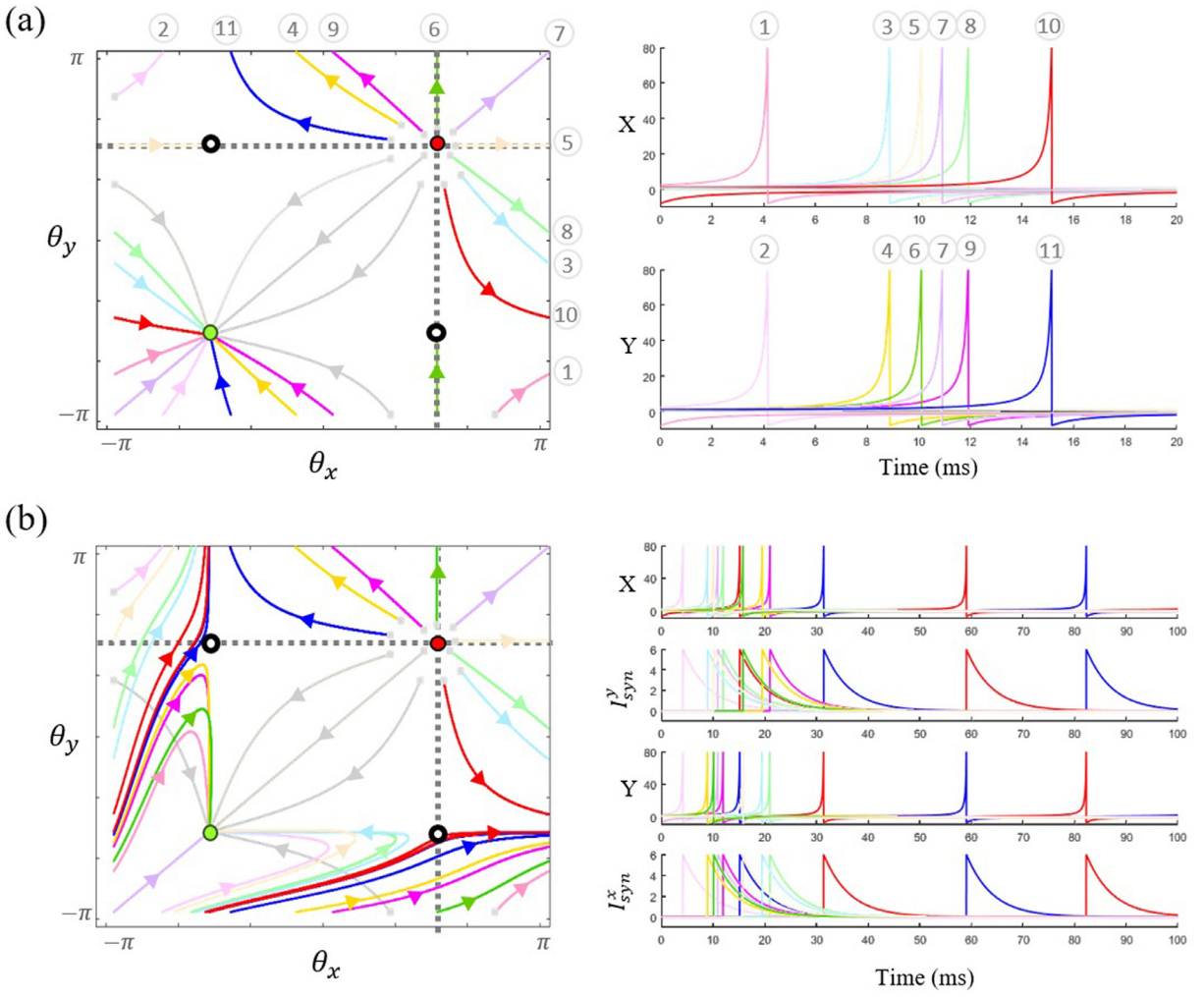

Fig. 2. Phase portrait and the corresponding signals of the network ($I_{ext} = -1$) in the time domain. In all of the left panels, the gray squares indicate the arbitrary initial states of the system; green circles indicate the stable fixed point; red circles, indicate the unstable fixed point; and the while circles indicate the saddle points of the network. Dashed black lines represent firing thresholds and separatrices of the unstable points. (a): On the left panel, 16 arbitrary initial states are considered to show the movements of the Phase variables for the uncoupled network ($J = 0$). The resulting membrane voltages in the time domain are shown with similar colors on the right and spike moments are specified with numbers both on the time domain and the phase portrait. In this uncoupled setting, neurons are excitable and as long as their voltages are under the threshold, they are attracted by the stable rest (gray curves). The other colored trajectories which initiate beyond the threshold, move toward the edges of the phase plane, make an action potential, reset back and enter from the other side of the plane to be attracted by the stable rest. (b): Similar 16 arbitrary initial states are considered to show the dynamical properties of the coupled network, with $J = 6$. In this setting after each spike emission, a time decaying synaptic current is produced that pushes the phase trajectories of the other neuron toward the separatrices. On the right side, the resulting signals of synaptic currents and action potentials are shown in the time domain, illustrating that except the red, and blue curves, all of the conditions have ended up in the stable rest. (c) On the left side, phase portrait of a similar coupled network is shown, in which an appropriate initial state ($X(0)$ =1.01 and $Y(0) = -8$) have soon derived the phase variables toward the stable limit cycle (SLC). The SLC is shown with solid black line, and the dashed line depicts the transient move from the initial state to the SLC. The spike trains corresponding to the orbits on the left, plus the synaptic currents provided by each cell toward the other, are plotted on the right. (For interpretation of the references to color in this figure legend, the reader is referred to the web version of this article.)

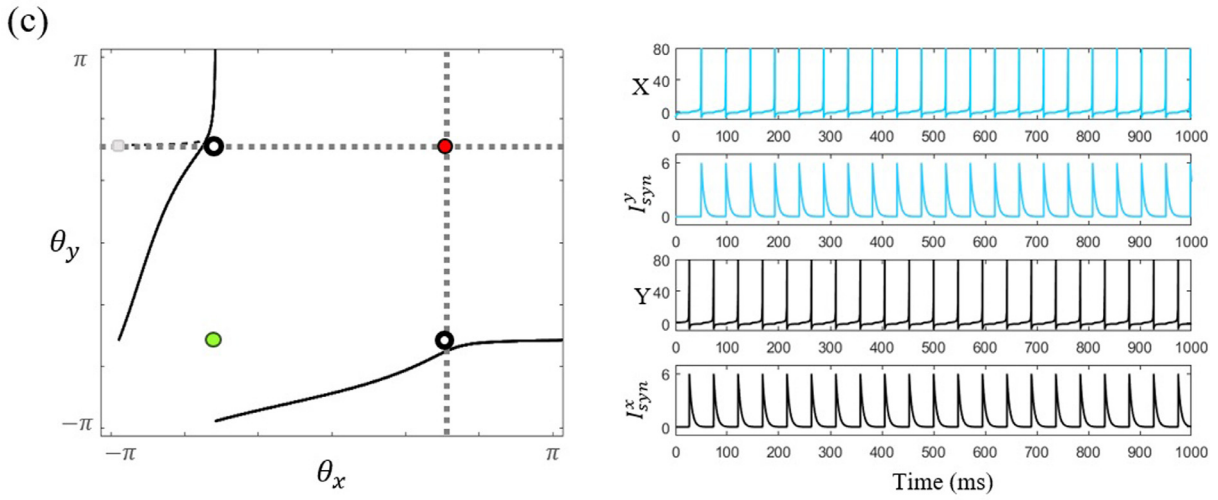

Fig. 2. Continued

they move toward the white unstable nodes as a result of the arriving synaptic currents. If the synaptic current arrives on time to force the membrane voltage crossing its threshold, another spike can be emitted.

When the neurons are synchronized, for example in the purple trajectory starting on the upper right region of this figure, the produced synaptic currents would arrive simultaneously to both neurons, when they are very low at their reset point, and later on their refractory periods. As a result, a small J, would not be able to turn the neurons on again. Even if the neurons are just partially synchronized, as in the pink trajectories (one of them starting at upper left and the other at lower right region), the same effect would lead to termination of the decaying synaptic current, before it can cause the other neuron to reach its threshold. one can see two trajectories (red and blue), that have been able to enter the bistable activity mode, and reach the stable limit cycle for producing a persistent pattern of firing. However, although the other seven trajectories which started somewhere close to the unstable node have succeeded in producing a second spike in the network, their activities have, after a short time, ended up in the stable rest.

The stable limit cycle, and the patterns of spikes and synaptic currents, are clearly shown in Fig. 2(c). In this panel, the network that we are going to study, is working noise-free at the first selected parameter pair ($J = 6$ and $I_{ext} = -1$). As discussed before, it has four equilibria at: $(+1, +1)$, $(+1, -1)$, $(-1, +1)$, and $(-1, -1)$. The latter is the stable fixed point, indicated with a green circle. The first one is an unstable fixed point, indicated with a red circle, and the other two are both saddle points of the network, indicated with while circles.

Moreover, as it was explained in the Methods, this network is bistable and in addition to the stable node, it has a stable limit cycle solution (SLC). In the left panel of Fig. 2(c) this SLC is illustrated with a solid black curve. The cyan square indicates the initial state of the system, which is chosen to keep the neurons at an appropriate antiphase mode leading to bistability. This initial state ($X(0) = 1.01$ and $Y(0) = -8$) soon evolves toward the SLC with a short transient move depicted with a dashed line in the figure. One second of corresponding spike trains and synaptic currents for both neurons, when the system works on its limit cycle is also shown on the right.

3.2. Noisy network and ISR

The two attractors of system (3), i.e. the SLC and the stable rest, have their own attraction domains with boundaries that divide the phase plane in to two regions; silent and active mode. Since the system coupled with time-dependent synapses is non-autonomous, the basins of attraction are time variant (see Section 3.4 for further discussion and Fig. 11 for examples of these varying borders).

We know that in the active mode, random perturbations can push the trajectories off the limit cycle and thus the bigger the amplitude of noise is, the more likely are phase variables to escape the SLC, cross the boundary, and dislocate into the attraction domain of the stable node. On the other hand, a network already in the silent mode is maybe perturbed towards the SLC, and start oscillating due to the force of random perturbations, provided the noise is strong enough to push the phase trajectories into the attraction domain of the limit cycle. These two phenomena are the foundation of ISR in bistable systems.

In Fig. 3, the effect of four different noise levels on the course of phase trajectories and the corresponding spiking patterns are illustrated for some arbitrary trials in a network with $I_{ext} = -1$ and $J = 6$. The temporal output of each neuron is recorded for a duration of $T = 1$ s and the noise onset moment is set at $t = 200$ ms. In panel (a), in spite of the fact that small perturbations ($\sigma = 0.1$) have made membrane potential trajectories make small detours from the SLC, neurons have

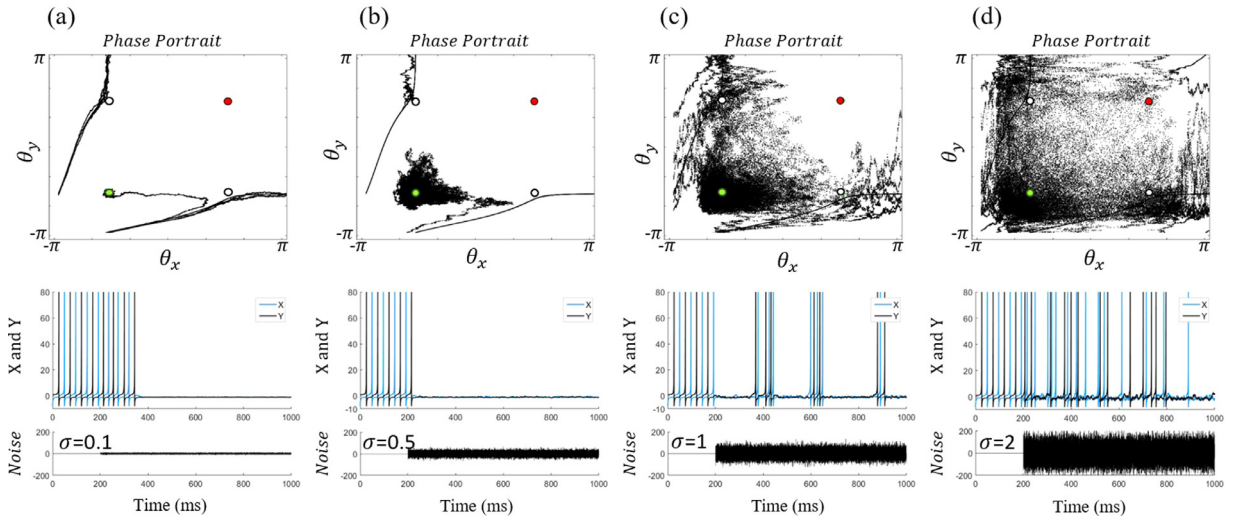

Fig. 3. The effect of four different noise levels on the persistent firing activity. First row: Phase portraits of the networks receiving noise. The green circle indicates the stable rest, the red circle indicates the unstable node, and the white circles indicate the saddle points of the system. Initial transient moves are removed from the orbits in these phase planes. Middle row: corresponding spike trains of the comprising components, (blue for X and black for Y). Bottom row: The white noise applied to the system. In all of the cases the network is initially at the persistent activity mode, producing a regular pattern of spiking. Then four different noise arrive at $t = 200$ ms and make the phase trajectories detour from the SLC. (a): A small noise with $\sigma = 0.1$ has switched the activity off at $t = 350$ ms. (b): A median noise with $\sigma = 0.5$ has soon stopped the activity after its arrival and never turned it on again (c): A noise with $\sigma = 1$ has soon switched the activity off, but it is large enough to bring the trajectories back to the SlC and irregularly form several action potentials. (d) A big noise of size $\sigma = 2$ has randomly moved the trajectories back and forth between the stable rest and the SLC, resulting in a stochastic pattern of spiking. (For interpretation of the references to color in this figure legend, the reader is referred to the web version of this article.)

continued firing for about 150 ms after the noise arrival, even though irregularly. Finally, the orbit is attracted by the stable fixed point and persistent activity has switched off at about $t = 350$ ms. We note that the network does not return to the active state in longer simulations (not shown).

In panel (b) of Fig. 3, the deviation from SLC, due to a medium level of noise (σ=0.5), is sufficiently large that after the noise onset moment, only neuron Y emits only one more spike before the activity stops. For the last two cases, in panels (c) and (d), where the noise amplitude is large, ($\sigma = 1$ and $\sigma = 2$), the system has moved several times back and forth between its attractors, switching on and off intermittently.

This process in a bigger picture introduces the ISR phenomenon. The U-shaped functions of Fig. 4 indicate the occurrence of ISR for twelve networks at different parameter points, taken from Table 1 and Fig. 1. Panels (a) to (d), correspond to the conditions at the global bifurcation border, and panels (e) to (l) relate to the further points upward in the parameter space. As it is observed, for all of the cases, there exist an intermediate range of noise which optimally terminates persistent firing, such that going either leftward or rightward from the middle, MFR is increasing.

In this figure the upper and the lower bounds of the shaded areas, indicate the maximum and minimum of MFR among 1000 trials. Wherever the shaded area has touched the x-axis, the activity had been terminated with no return to activity, at least once among all trials. In addition, as the main MFR curve (dark blue) moves upward, the percentage of trials in which the activity had been totally switched off decreases. Therefore, ISR curves of panels (e) to (l) suggest that termination of persistent firing by noise, is less likely when getting farther from the global border of bifurcation. These effects of noise, had been reported in the pairs of coupled Type 1 neurons [31,33,34], Morris-Lecar neurons [46], Hodgkin–Huxley neurons [19,32,47] and in large populations of networked spiking neurons [48]. Details of the dynamical structures which lead to these effects had been also propounded in [37].

An appreciable feature in Fig. 4 that had not been discussed in previous studies, is the gradual growth of the ISR's concavity width from panels on the left to panels on the right. In fact, the farther the neuron pairs are from the mono-stable oscillatory region of activity, the wider are the ISR curves, and thus the more difficult is transition from the silent to the active mode.

We argued that the required J for switching on the persistent firing depends on I_{ext}. With the same analogy we suggest that the required energy to move from the silent to the active mode by the noise, also, depends on the value of external current. The more negative the external current is, the bigger will be the concavity width in the mean firing rate. (Comparing the basins of attraction when moving from the stable fixed point to the SLC that are numerically computed and illustrated in Fig. 9 of Section 3.4, supports this fact).

Furthermore, getting farther above the synaptically induced bifurcation, makes the SLC more robust. As depicted in Fig. 4, panels (e) to (l), in contrast to panels (a) to (d), Mean Firing Rate (MFR) of the networks, does not fall abruptly with noise, and rarely reach zero, when working farther from the global bifurcation. By robustness we mean that a small

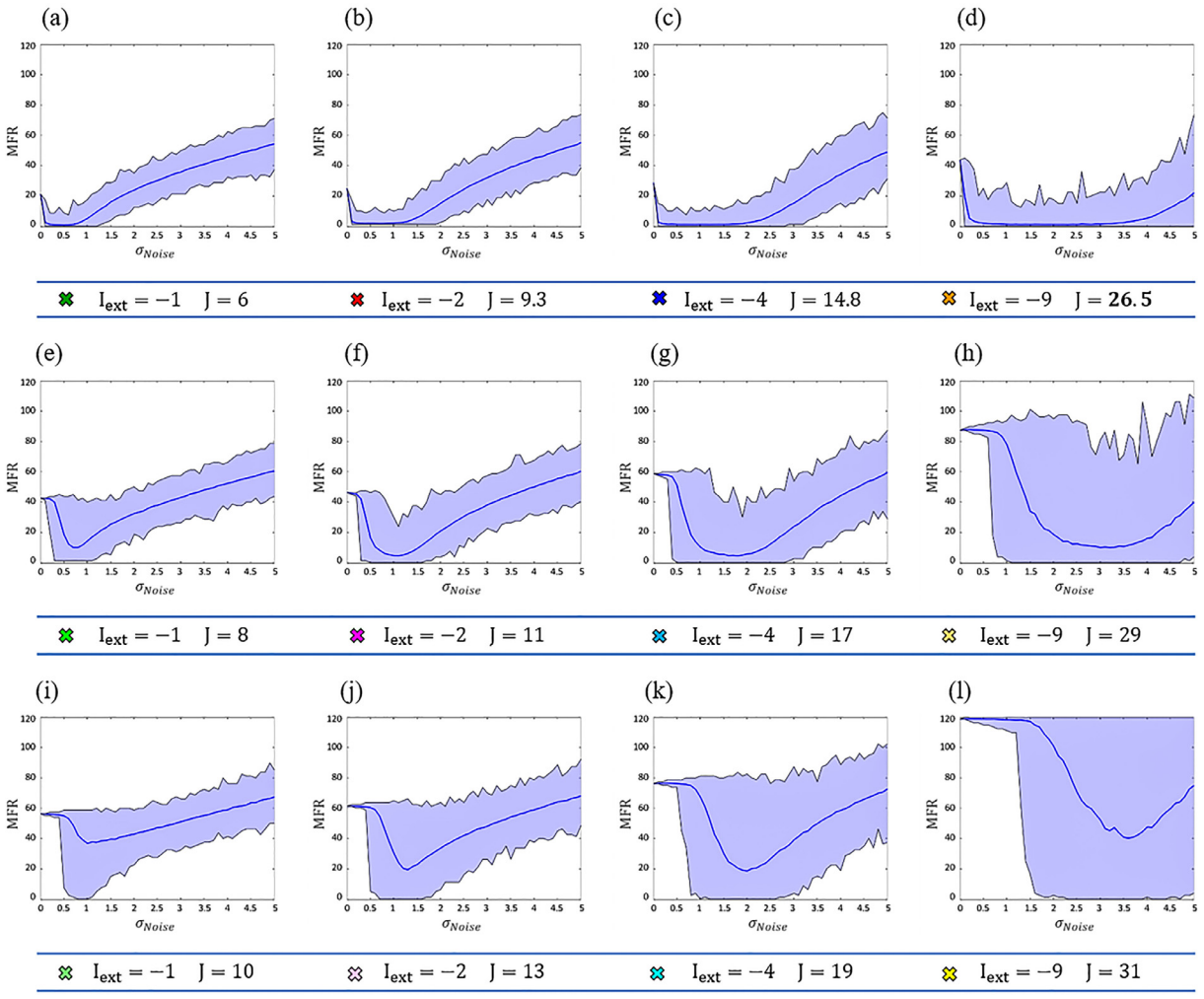

Fig. 4. Mean Firing Rate (MFR) versus the noise intensity, forming U-shaped ISR curves at 12 different parameter points. Corresponding parameter values are written under each case, and indicated with colored crosses as marked in figure and Table 1. The first row shows ISR, at four points on the border of global bifurcation, illustrating that SLC is extremely fragile there. The networks' MFRs fall down with tiny noise and neurons remain off (MFR = 0) at median noise levels. The second and third rows relate to the cases farther from the global bifurcation border. This getting farther has increased the minimums of MFR, and their falling slope, suggesting that the SLCs become more and more stable, decreasing the probability of stop. Upper and lower bands of the shaded areas illustrate the maximum and minimum of firing rate among 1000 trials. Moreover, the range of noise which keeps the network silent expands from panels on the left to panels on the right, (corresponding to the parameter pairs from right to the left of Fig. 1). (For interpretation of the references to color in this figure legend, the reader is referred to the web version of this article.)

noise has a low chance for terminating the activity. Considering this effect is of interest, when modeling bistable neural network oscillators that are supposed to be sensitive to, or robust against noise.

3.3. Stochastic resonance

We hypothesize that in the presence of noise with amplitude at the level optimal for inducing ISR, the network's ability to represent external stimuli would be also optimal. Indeed, in this condition, the synaptically sustained firing of the network, is prone to terminate, so the comprising neurons are primed to response to the external stimulus. As a result, an optimal intermediate noise level, which is not strong enough to push the system from the silent to the active mode, would add up to the weak external stimuli and excite neurons so that the resulting firing pattern will be indicative of the input's time structure. In summary, we propose that the ISR can produce conditions for SR. This hypothesis, is tested at two different conditions: in first we project the temporally structured spiking input from the third neuron to both neurons in the network; and in the second the input is projected to only one of the neurons and we use the unstimulated neuron in the network as the read out. The circuit schematic diagrams of these two conditions are shown in Figs. 5(a) and 6(a) respectively.

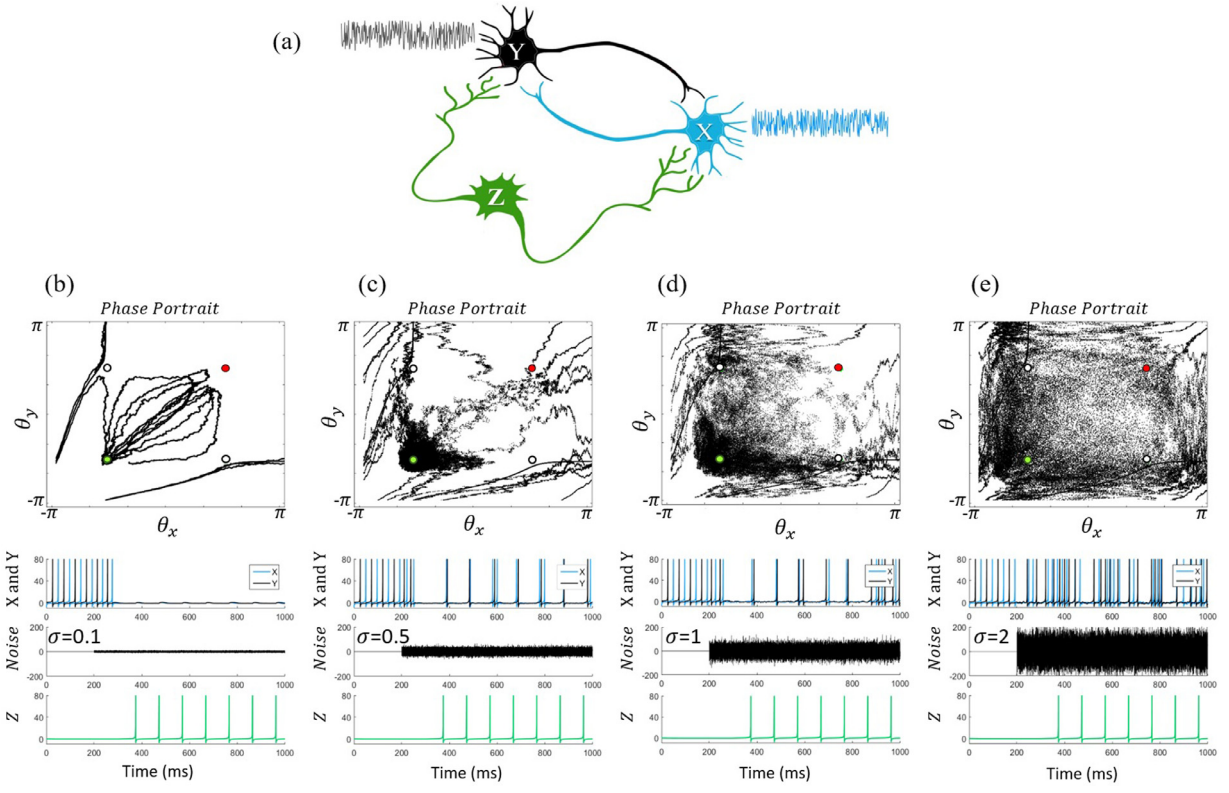

Fig. 5. The network's reaction to the external input, in the presence of four different noise levels, when Z is connected to both X and Y. (a): Schematic of the original network comprising two identical neurons, X and Y, that are synaptically coupled. Except from the synaptic currents that these neurons receive from each other, they receive an identical tonic input from a third neuron, Z, plus an independent signal of white noise, externally. The first row below this schematic diagram: Phase portraits of the networks receiving noise and Z signals. The green circle indicates the stable rest, the red circle indicates the unstable node, and the white circles indicate the saddle points of the system. Initial transient moves are removed from the orbits in these phase planes. Second row: Corresponding spike trains of the comprising neurons (blue for X and black for Y). Third row: The white noise applied to the system at $t = 200$ ms. Last row: The spiking pattern of neuron Z, starting at $t = 350$ ms. In all of the cases the network is initially at the persistent activity mode, producing a regular pattern of spiking. (b): A small noise with $\sigma = 0.1$ has switched the activity off and although the input signals have moved the phase trajectories from the stable rest toward the diameter of the plane, they could not bring the system back to the active mode. (c): A median noise of size $\sigma = 0.5$ has terminated the activity, but later the input signals with the help of this noise could push the trajectories to the attraction domain of the SLC, and result in a firing pattern that has the Z temporal information in it. (d): Similarly, a noise signal with $\sigma = 1$ has first terminated the activity and then helped the input signals to push the trajectories reaching the SLC and producing e a spiking pattern which reflects the Z time structure. (e): A big noise with $\sigma = 2$, has randomly driven the phase trajectories on the phase plane, resulting in a stochastic pattern of firing. The effect of Z signals is not discernible here. (For interpretation of the references to color in this figure legend, the reader is referred to the web version of this article.)

First, Fig. 5 illustrates the response behavior of the network in reaction to the external input, for three arbitrary trials where Z is stimulating both X, and Y. And second, Fig. 6, illustrates the condition where Z is feeding the network, only through X. In both conditions the networks are left noise-free for the first 200 ms, and then two independent signals of white noise are injected to neurons X and Y. Later at the time point $t = 350$ ms, neuron Z is switched on to feed the original network, externally.

Panel (b) of Fig. 5 demonstrates that a short while after the onset moment of a small noise ($\sigma = 0.1$), persistent firing has switched off, and has never turned on again. Although the basins of attraction are not known here, the phase portrait's image clearly signifies that the force of external currents coming from Z, plus noise, have propelled the trajectories on the diameter of the plane, but have never been able to force them crossing the boundary and ending up in the attraction domain of the SLC (Attraction domain of SLC is shown in Fig. 9).

On the contrary, in panels (c) and (d) of the same Fig. 5, after termination of persistent firing by the force of the median noise ($\sigma = 0.5$ and $\sigma = 1$), external inputs coming from Z, with the help of random perturbations, are able to push the phase trajectories from around the stable rest, toward the SLC, and evoke spikes. As a result, the output pattern of firing reflects the time structure of the input. Lastly, in panel (e), where the noise amplitude is bigger, ($\sigma = 2$), the irregular spiking pattern of X and Y is driven by the noise and does not appear to carry information about Z.

Similar results are also observable for the second condition, in Fig. 6, where Z is stimulating the network only through neuron X. Here, in contrast to Fig. 5, the phase trajectories do not move through the diameter of the plane, but they mostly move on the X-axes. As a result, neurons are not greatly synchronized by the input, and the temporal information of Z,

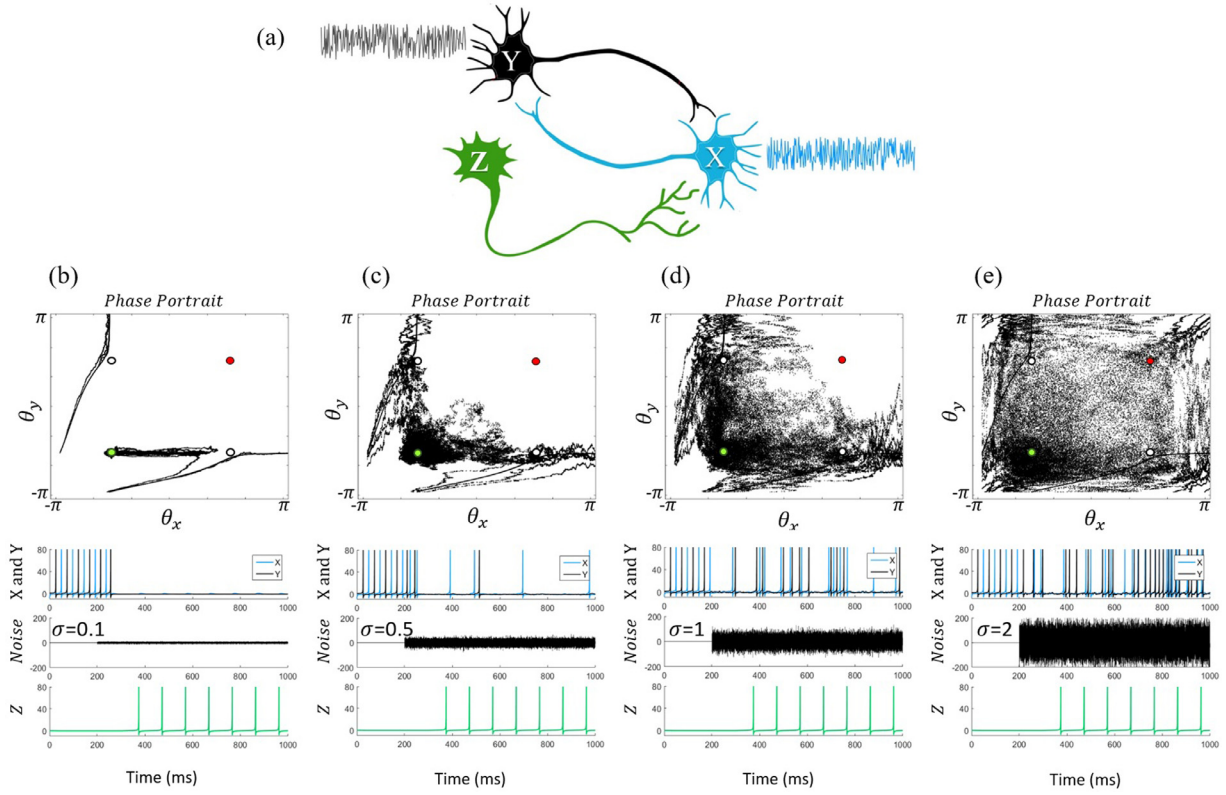

Fig. 6. The network's reaction to the external input, in the presence of four different noise levels, when Z is only connected to X. (a): Schematic of the original network comprising two identical neurons, X and Y, that are synaptically coupled. Each neuron receives a synaptic current from the other one and an independent signal of white noise, externally. Neuron X, receives an extra tonic input from a third neuron, Z. The first row after this schematic: Phase portraits of the networks receiving noise and Z signals. The green circle indicates the stable rest, the red circle indicates the unstable node, and the white circles indicate the saddle points of the system. Initial transient moves are removed from the orbits in these phase planes. Second row: Corresponding spike trains of the comprising neurons (blue for X and black for Y). Third row: The white noise applied to the system at $t = 200$ ms. Last row: The spiking pattern of neuron Z, starting at $t = 350$ ms. In all of the cases the network is initially at the persistent activity mode, producing a regular pattern of spiking. (b): A small noise with $\sigma = 0.1$ has switched the activity off and although the input signals have moved the phase trajectories from the stable rest, toward the repeller of neuron X, they could not cross the threshold and make a spike in the network. (c): A median noise of size $\sigma = 0.5$ has terminated the activity, but later the input signals with the help of this noise could cross the threshold of X and cause several spikes that reflect the Z temporal information. In this condition, neuron X has a higher chance of spiking, since it is directly connected to Z. There is only a single spike produced by neuron Y here. (d): Similarly, a noise signal with $\sigma = 1$ has first terminated the activity and then helped the input signals to push the trajectories reaching the SLC and producing a spiking pattern which reflects the Z time structure. (e): A big noise with $\sigma = 2$, has randomly driven the phase trajectories on the phase plane, resulting in a stochastic pattern of firing. The effect of Z signals is not discernible here. (For interpretation of the references to color in this figure legend, the reader is referred to the web version of this article.)

carried to neuron X, is stronger than the received information by neuron Y. This fact, may be understood by looking at the spike patterns of Fig. 6, in panel (b). It is observed that X (blue), has a higher chance of spiking compared to Y (black), since it is directly connected to Z. However, it will be shown that even in this condition, the information transfer to Y, will be maximized at a median noise level.

Examining Figs. 5 and 6 closely, we can see that the evoked spikes in the network have a short time delay with respect to the Z signals. This effect, and the SR phenomenon in general, are clearer collectively at multiple trials as illustrated in Fig. 7. In this figure, the same simulations as had been performed for Figs. 5 and 6, are repeated a hundred times, to study the effect of various noise levels on the firing pattern of the network, comparable with the time structure of the stimulus. The first boxed row, indicated with "I", corresponds to the raster plots of X and Y, when they are simultaneously receiving the Z signal, and the second box, "II", corresponds to the case where Z is only connected to X. In panel (a), during the period that a small noise with $\sigma = 0.1$ is present, before the stimulus arrival, X and Y tend to spike irregularly. Such irregularity is higher in panels (c), (d), and (e) due to the presence of bigger noise, compared to panel (a). In panel (b), instead, the persistent activity has most often terminated soon after the noise onset moment, which is a result of the ISR. Later, when the external input, Z, starts at about $t = 350$ ms, we can see a signature of it in the raster plots of X and Y. Arguably, the information transfer in panel (a) is not very successful, but we can see that in the panels, (b) and (c), the time pattern of Z, is apparent among the X and Y's spiking behavior. In these conditions a high level of Mutual Information between X (or Y) and Z is expected. For the bigger noise levels, in panels (d) and (e) also, the transferred information from Z to the network

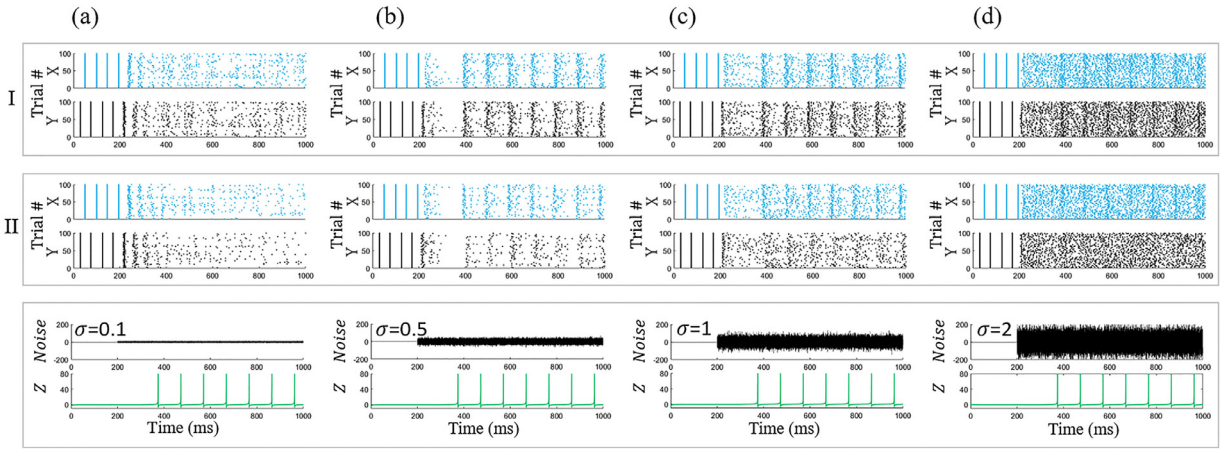

Fig. 7. Raster plots of X and Y at two different conditions; *I*: Z connected to both neurons, and *II*: Z connected to X, only. The applied white noise at $t = 200$ ms, and the spiking pattern of neuron Z (green), starting at $t = 350$ ms, are shown in the third box. In all of the cases the network is initially at the persistent activity mode, producing a regular pattern of spiking. (a): A small noise with $\sigma = 0.1$makes the collective spiking pattern irregular, before the input arrives. The density of raster plots decreases through time, suggesting that the noise is switching off the activity in many trials. This decrement is most clear in the raster plot of neuron Y in the box II, because in that condition Y is less affected by Z, and is mostly under the noise control. (b): A noise of size $\sigma = 0.5$ has switched off the persistent activity in almost all of the trials, before Z arrives. Then the input signal has reflected its temporal pattern in the X and Y spiking behaviors. This information transfer is stronger in box I rather than box II. (c): A noise signal with $\sigma = 1$ has caused a sparse collective spiking pattern in the network before the input arrives. However, later the input signal has organized the spiking patterns in a way that its temporal information is reflected in the network behavior. Similar to the other case, the information transfer is stronger in box I rather than II. (d): A big noise of size $\sigma = 2$, has led to a random spiking pattern such that in contrast to other cases, the time pattern of Z signal is hard to discern in the raster plots. (For interpretation of the references to color in this figure legend, the reader is referred to the web version of this article.)

is hard to discern. It seems that the ubiquitous noise-induced spikes, have attenuated the process of information transfer. It will be shown that this effect will lead to the reduction of MI. Furthermore, as expected, in the box I, where stimulus is injected to both neurons, the visible Z pattern within the raster plots of X and Y seems very similar, while in the box II, the Z pattern is more clear among X spikes, rather than Y. (Figures of the raster plots with higher noise levels as well as the noise-free conditions are provided in the supplementary, figure SIV)

In order to quantify how the external signal structure is transmitted from Z to the network, at different noisy conditions, we computed the average of Mutual Information, MI_{mean}, measured over 2000 trials for each noise level and results are plotted in Fig. 8. This figure demonstrates that MI between the network firing behavior and the input signal has a peak at an intermediate noise strength, manifesting Stochastic Resonance (SR). In other words, the network's ability to process and represent the time structured input Z, is maximal when a noise source with an intermediate strength is present. In general, we suggest that SR in information transfer, is a direct consequence of ISR in the endogenous firing. Thus, it is expected that the main features of the ISR curves, such as their general shape, depth and width, correlate with the features of the SR curves.

Investigating different panels of Fig. 8, first of all, demonstrates that the transferred information to X and Y, in the case of simultaneous stimulation of both neurons (Dashed green and red lines) have similar shapes and amplitudes everywhere. However, in the second case, where the stimulus is only injected to X and its information indirectly transfers to Y through the coupling, the MI functions for X and Y have different amplitudes, even though they still have similar bell shapes. In fact, in this condition, since neuron X is more strongly synchronized with neuron Z, its relative MI values (Solid green lines) are always larger than the MI values of Y (Solid red lines).

Second, we can see that as the ISR curves (Solid blue lines) widen by going leftward on the parameter space, the corresponding SR curves also grow their width, respectively. This effect is most clear when comparing panels (a) to (d) and panels (e) to (h) of the Fig. 8. In the panels of the last row, however, the parameter points are too far from the global bifurcation border that the SR effect is not easily trackable. In panels (j) and (k) the noise-induced activities at the middle of the curves have the mean firing rates (MFR) of approx. 20 Hz, which is a low enough rate to let the Z signal to be represented at the median noise levels, even though weakly. In panels (i) and (l), on the other hand, the noise-induced activities have formed minimum MFRs of about 40 Hz, in the middle of the curves. In these conditions, the high rates of the network firing, do not allow the Z inputs to be reflected in the X and Y spiking patterns, and thus SR is almost absent.

Next, we quantified the efficacy of the information transfer as a function of the distance of the specific parameters of the network from the border of the global bifurcation (the onset of network synaptically-induced bistability). Each column of Fig. 8 relates to a given value of external current, such that the panels in the first row correspond to the parameter pairs on the border of global bifurcation, and the lower panels of the second and the third row are for parameters getting progressively farther from the bifurcation line. Comparing the maximum values of MI, at the peaks of the SR curves, between the panels of each column, suggests that for an identical input received by bistable networks of various parameters, the

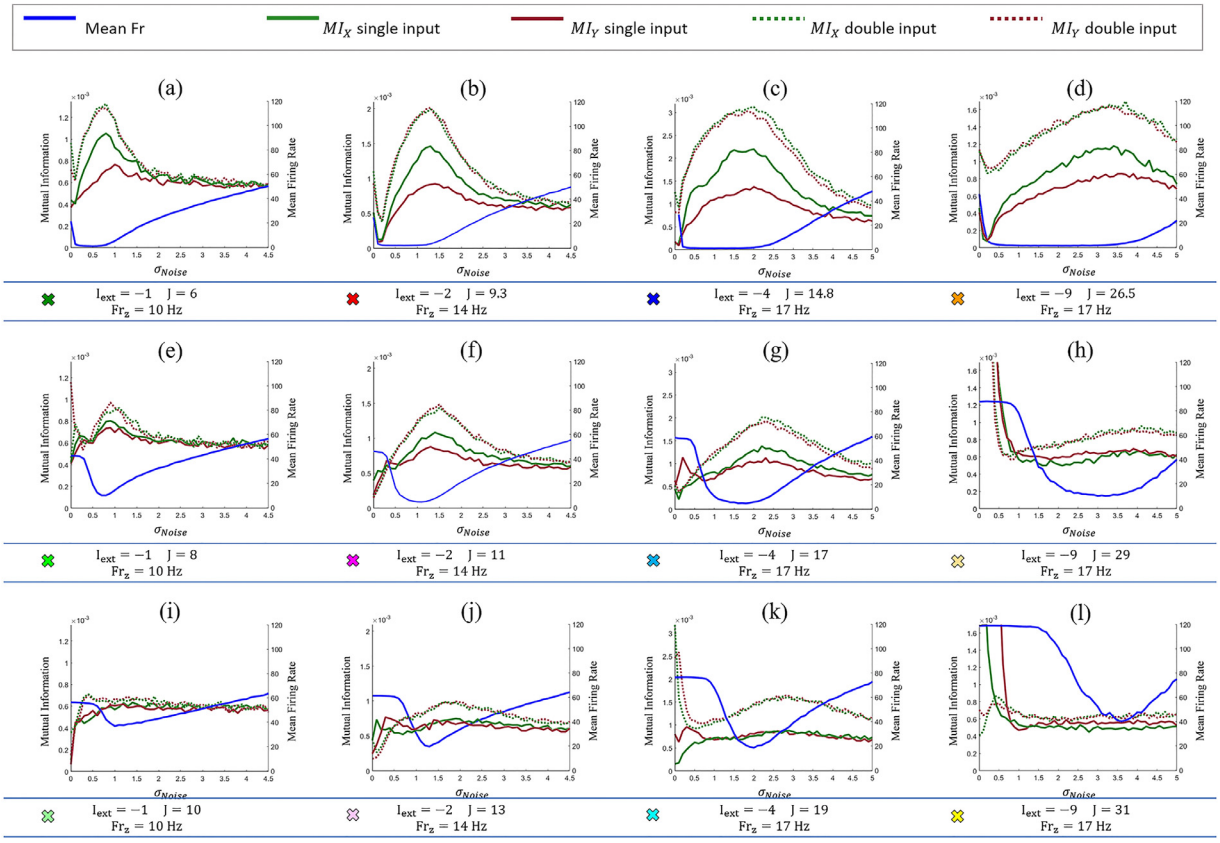

Fig. 8. ISR and SR curves plotted together for the networks at 12 different parameter pairs. Corresponding parameter values are written under each case, and indicated with colored crosses as marked in Fig. 1 and Table 1. The first row shows SR versus ISR, at four points on the border of global bifurcation, and the second and third rows relate to the cases farther from the bifurcation border, upward in the parameter space. Solid blue lines indicate the U-shaped ISR curves. Dotted green (red) lines indicate the SR curves of neuron X (Y) related to the case where Z is connected to both X and Y. Solid green (red) indicate the SR curves of neuron X (Y) related to the case where Z is connected to X, only. (For interpretation of the references to color in this figure legend, the reader is referred to the web version of this article.)

closer the network is to the bifurcation border, the stronger SR will occur in that. This effect is, as expected, similar to the decrement of the ISR depths, when going farther from the bifurcation. Moreover, as we can see in panels (h), (k) and (l), as the endogenous firing rate of the network grows, the ISR effect decreases and a peak at the noise-free condition arises in the MI curves. The dynamical mechanisms which lead to the formation of these peaks, and differences of this effect for the single-input and the double-input cases remain an interesting topic for future studies.

Table 2 indicates the obtained optimal values of noise for SR and ISR, as well as the optimal MIs, and optimal MFRs, at those critical noise levels. Here MI_{max} values are only shown for the double input cases, where the MI at X and Y are mostly equal. In the case of small differences, the average value is shown in the table. Likewise, about the optimal noise levels, wherever a small difference is observed at the SR curves of X and Y, the average value is reported.

3.4. Dependence of ISR and SR on network dynamic parameters

The main finding of this work is the fact that wherever a bistable reciprocally connected spiking neural circuit reveals ISR in its endogenous behavior, it will also show SR, provided an external input is to be represented by the system. The key is that the noise amplitude tuning of the ISR, coincides with the tuning of the SR.

ISR curves, have three main characteristics, which are investigated in this section: (1) the concavity width, (2) the concavity depth, and (3) the falling slope of MFRs. Variations of the ISR's concavity width and concavity depth at different parameter regions, which directly affect the SR characteristics as well, are about the properties which lead to termination of persistent firing. Thus, to interpret these variations, the structure of attraction domain when moving from silent to the active mode must be known. However, when the ISR curve is descending from the endogenous firing rate toward the minimum MFR (left half of the curves), the system is in fact moving from the active to silent mode (collapsing onto the stable steady state). If we want to investigate why the falling slope of the curves vary at different conditions, it is necessary to consider the attraction domain structures when moving from the active to the silent mode.

Table 2
Numerical results of the SR and ISR features.

Point mark	✖	✖	✖	✖
$FR_{noisefree}$ (Hz)	20	25	30	40
MFR_{min} (Hz)	0.83	1.87	1.14	1.09
ISR : $\sigma_{optimal}$	0.5	0.7	0.9	2.3
SR : $\sigma_{optimal}$	0.8	1.3	1.9	3.5
MI_{max} (Double input)	1.3	2	3	1.6
Point mark	✖	✖	✖	✖
$FR_{noisefree}$ (Hz)	42	45	58	87
MFR_{min} (Hz)	10	4.6	4.5	10
ISR : $\sigma_{optimal}$	0.75	1.1	1.8	3.2
SR : $\sigma_{optimal}$	1	1.5	2.3	4
MI_{max} (Double input)	0.9	1.5	2	0.9
Point mark	✖	✖	✖	✖
$FR_{noisefree}$ (Hz)	55	60	76	118
MFR_{min} (Hz)	36.8	19.5	18.5	40
ISR : $\sigma_{optimal}$	1	1.3	2	3.6
SR : $\sigma_{optimal}$		1.8	2.8	
MI_{max} (Double input)		1	1.6	

Since the connecting synapses are non-autonomous (they depend on time explicitly), the attraction basins change their shape at different time points, and make it impossible to identify them analytically. However, as long as the system remains on its stable node, the attraction basins of the SLC are static, and numerically computable. In addition, as long as the system is working on its SLC, the attraction basins of the rest state can be accessed at some discrete time points within the network's course of action. Applying numerical methods for estimating the borders of attraction at several consecutive moments, can provide appropriate information about the evolution and the generic form of these borders.

Starting with a silent network, we can numerically map out the areas of the phase plane such that moving X and Y to them from the stable rest, will switch the system to the persistent activity mode. In this condition, the structure of the attraction basins would be different from what had been obtained previously, because the system behavior depends on the time point at which the phase trajectories are kicked toward different destination points on the plane. That is, in fact, due to the presence of time decaying synaptic currents in the network. These synaptic currents can sustain the persistent activity in face of the perturbation (depending on the perturbation timing and amplitude) and prevent its termination. Consequently, a destination point that had been assigned to the attraction domain of the stable rest previously, may belong to the attraction domain of SLC this time.

First, to identify the SLC attraction domain we start the system in the silent state and numerically determine the border in the phase space where the trajectories must cross in order to dislocate in to the persistent firing mode. Therefore, when the system is off, an external impulse is designed to move the phase variables from the stable fixed point (both neurons at rest), toward a new point in the phase plane. Then the network is simulated to determine if it starts spiking, or returns to its rest state. In the first case, the destination point can be assigned to the attraction domain of the SLC; and in the latter

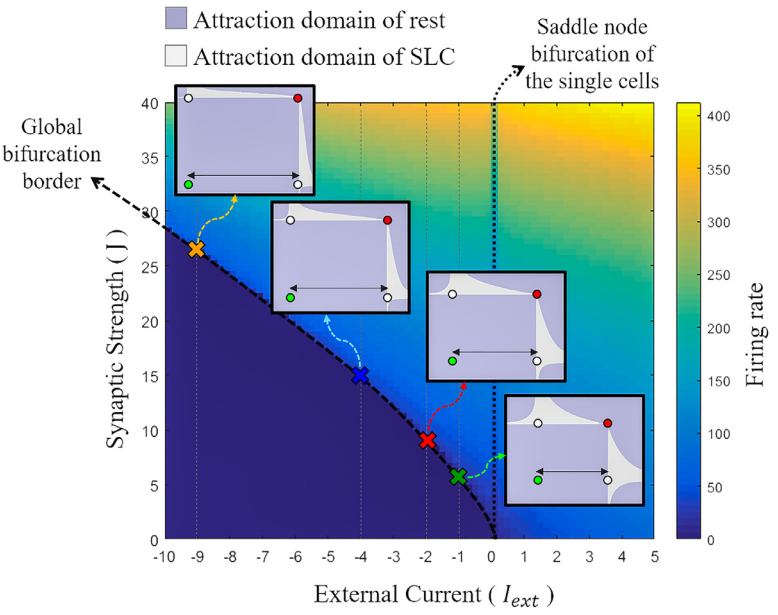

Fig. 9. Attraction domains of the stable rest and the SLC, as a function of the network's distance from the border of single neuron's saddle node bifurcation. The large picture is the parameter space of the coupled network in which the firing frequencies, relative to each parameter pair, (I_{ext} , J), are color coded and shown on the right-side bar. The colored crosses indicate four points on the border of global bifurcation that their corresponding phase portraits are plotted in the inner boxes, connected to related point with colored dashed lines. In these inner boxes, the green circles indicate the stable rest, the red circles indicate the unstable node, and the white circles indicate the saddle points of the system. Gray regions are the attraction basins of the SLC, and the light purple regions are the attraction basins of the stable rest, which are found numerically when the network is kicked from the rest point to 20,449 different destination points on the phase plane. It is shown that getting farther from the single neurons' saddle node bifurcation, expands the distance between the stable rest and the attraction domain of the SLC, which in turn would lead to requirement of a larger energy for crossing this distance and moving to the active mode from the rest state. This feature of the phase portraits, reasons the expansion of SR and ISR widths, from the right side to the left side of the parameter space. (For interpretation of the references to color in this figure legend, the reader is referred to the web version of this article.)

case, to the attraction domain of the fixed point. By executing this procedure at 20,449 (143 $\times$ 143) different destination phase points on the phase plane, we can estimate the shape of the attraction basins.

Each inner panel of Fig. 9, indicates the phase portrait of a network close to the global bifurcation border. The gray areas demonstrate the attraction domain of the SLC, while the light purple areas indicate the fixed point's attraction basins. The parameter values which are employed to obtain this figure, are the same as the network parameters which were used in panels (a) to (d) of both Figs. 4 and 8, (first four rows of Table 1). We showed there, that going leftward in the parameter space, leads to expansion of both SR and ISR widths. Also, we claimed that these widths depend directly on the value of the external current. To explain this effect, it is necessary to consider the fact that, concavity width of the ISR curves, as well as the convexity width of the SR curves, are related to the energy required for switching the activity back to spiking after it has stopped by the noise (in a sufficiently short period of time). The distance which must be crossed by the phase trajectories, for moving from the stable rest (green nodes) to the SLC's attraction domain (gray regions) at different parameter values can be compared in Fig. 9. It is clear that to the left of the parameter space this distance is larger than the cases on the right.

In fact, the required energy for switching the persistent firing on, is a direct function of the distance between the stable rest and the unstable node (threshold) for each neuron, which is in turn determined by the value of I_{ext}. Whether this energy is provided by synaptic coupling within the network, a synaptic current from an external source, or by random perturbations, the more negative the external current is, the larger energy will be required to cross this distance. Consequently, for the networks with more negative I_{ext}, the noise amplitude which the right half of the ISR curves rise at, will be greater. The optimal condition for the external inputs to be represented in the network's activity is when the endogenous firing is off. As a result, the noise amplitude to drop the right half of the SR curve will be bigger, when I_{ext} is more negative. That is why the curves in Figs. 4 and 8, expand from panel (a) to (d), and from (e) to (h).

Previously, we showed that moving upward in the parameter space, at a constant external current, will decrease the efficiency of ISR, that was manifested by decrement of the ISR curves' depth. This depth, which in turn correlates with the SR efficacy, is another property that can be elucidated using the static attraction domains, when moving from the silent to the active mode. The structure of these attraction basins are obtained for a system with fixed external current t $I_{ext} = -1$ and six different values of the synaptic strength, J $\in$ {5.8, 5.9, 6, 7, 8, 10}, illustrated in Fig. 10.

$J = 5.8$, corresponding to the lowest inner box of Fig. 10, is the smallest synaptic strength, at switch we can see bistability, but as it is observed, almost all of the phase plane in this condition is covered by the attraction domain of the fixed point

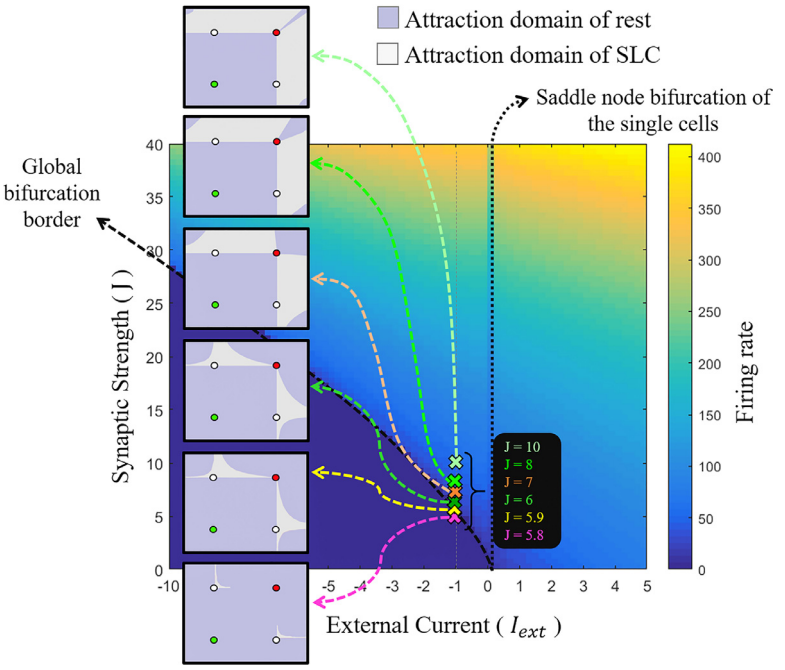

Fig. 10. Attraction domains of the stable rest and the SLC, as a function of the network's distance from the border of global bifurcation. The large picture is the parameter space of the coupled network in which the firing frequencies, relative to each parameter pair, (I_{ext} , J), are color coded and shown on the right-side bar. The colored crosses indicate six points on the vertical line $I_{ext} = -1$. The corresponding phase portraits of all of these points are plotted in the inner boxes, connected to their relative points with colored dashed lines. In these inner boxes, the green circles indicate the stable rest, the red circles indicate the unstable node, and the white circles indicate the saddle points of the system. Gray regions are the attraction basins of the SLC, and the light purple regions are the attraction basins of the stable rest, which are found numerically when the network is kicked from the rest point to 20,449 different destination points on the phase plane. It is shown that going upward in the parameter space, expands the SLC's attraction domain, which in turn would lead to easier attainment of shifting back to the activity mode, form the rest state, with random perturbations. This feature of the phase portraits, reasons the decrement of SR and ISR depths, from the bottom to the upper areas of the parameter space. (For interpretation of the references to color in this figure legend, the reader is referred to the web version of this article.)

(light purples region). Hence the region of the phase space from which the active state can be switched on is extremely limited. As shown in the other inner boxes, by receding from the border of network bifurcation, this region gradually grows, such that at some point ($J = 13$, not shown here), the gray region masks all the phase space beyond the separatrices of the saddle nodes (the white points, Fig. 10).

The probability that a random signal can bring a system which is at the fixed point, back to the active mode, depends on the area of the SLC's attraction domain: the larger the SLC's attraction domain, the more probable is the network to end up in the persistent firing mode. Heuristically, Fig. 10 suggests that going upward in the parameter space should increase this probability. For example, in the lowest panel where the network is right on the edge of the bifurcation border ($I_{ext} = -1$ and $J = 5.8$), the attraction domain of SLC (gray region) is extremely small and narrow. Therefore, the perturbations that attempt to randomly drive the trajectories on the phase plane, are not likely to fall (and rest) in that small region. Hence the transition to persistent activity should be low. Moving slightly upward on the same vertical line, as shown in the second panel ($I_{ext} = -1$ and $J = 5.9$) would lead to significant expansion of the SLC's attraction domain. As a result, the possibility of moving from the purple (silent) regions to the activity (gray) regions, by the force of noise, would be also greater. The other panels indicate that the expansion of the SLC's attraction domain by getting farther from the bifurcation border, continues until the gray region covers almost all the areas of the phase plane above the unstable nodes.

In short, noise, in a network further above the global bifurcation, has a higher chance of switching on the activity, compared to the conditions close to the global bifurcation border, such as the cases in Fig. 9. This dynamical property determines the critical point where MFR starts rising at the middle of the ISR curves. Indeed, when the chance of stochastically dislocating to the SLC attraction domain is high, the probability of persistent spiking at the presence of noise will be also high, and thus MFR would not decrees significantly. As a result, going farther above the global bifurcation border, increases the minimum MFR, and thus decreases the ISR depth. Interestingly, from the phase plane we can also see that noise that is perfectly correlated between the two neurons in the network cannot turn the activity from the rest to the SLC – an identical input noise will evoke a perfectly synchronous solution that is necessarily heteroclinic between the double saddle (threshold crossing by both neurons simultaneously) and the rest.

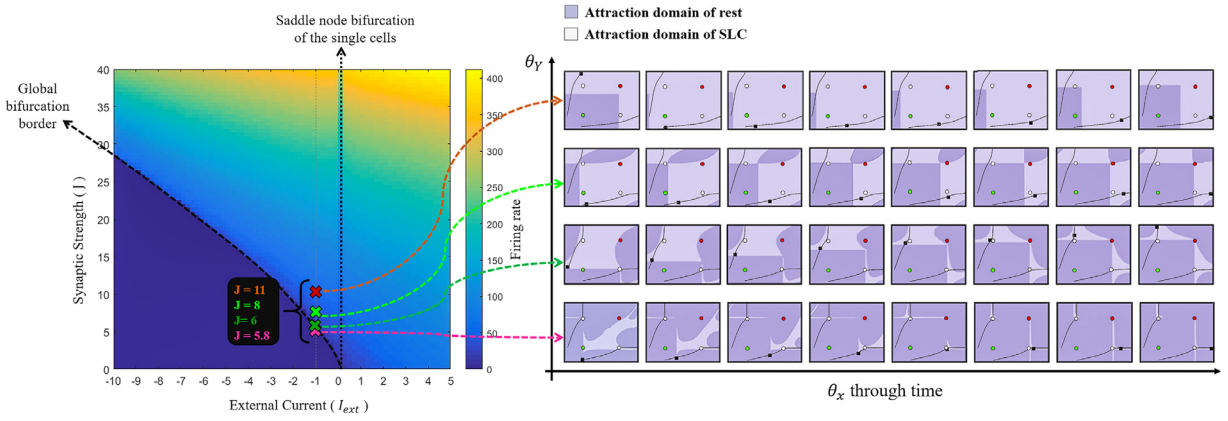

Fig. 11. The evolution of attraction domains through a limit cycle timespan, as a function of the network's distance from the border of global bifurcation. The right panel indicates the parameter space of the coupled network in which the firing frequencies, relative to each parameter pair, (I_{ext} , J), are color coded and shown on the right-side bar. The colored crosses indicate five points on the vertical line $\boldsymbol{I_{ext}} = -1$, from the border of global bifurcation to farther points upward in the parameter space. The corresponding phase portraits of all of these points are plotted in the boxes on the left panel, connected to their relative points with colored dashed lines. In these boxes, the four fixed points of the system and the SLCs are shown on the phase planes. blue regions are the attraction basins of the SLC, and the red regions are the attraction basins of the stable rest. In each row on the right panel, 8 different spots uniformly distributed on half of the SLC's period are chosen, and phase trajectories are kicked from those points to 20,449 different destination points on the phase plane. This way, the structures of the attraction domains are found numerically when the network is kicked from a point on the SLC to other regions of the plane. These selected points are indicated with small black squares on the SLC. It is shown that going upward in the parameter space, expands the SLC's attraction domain (averaged in time), which in turn leads to difficulty of switching off the persistent activity. This feature of the phase portraits, reasons that why the falling slope of MFR at the left half of ISR curves is steep close to the global bifurcation border, and gets shallower as going upward in the parameter space. (For interpretation of the references to color in this figure legend, the reader is referred to the web version of this article.)

The SR efficacy, or in other words, the maximum MI, will also decline when the system is far from the border of global bifurcation, because external inputs reveal themselves in the network activity only when the intrinsic MFR of the original non-driven network is low.

Finally, inspecting different panels of Fig. 4, suggests that the falling slope of the ISR curves, is inversely proportional to the J values. In the first row of this figure, where all of the considered conditions are almost on the border of global bifurcation, MFR falls down abruptly with very small perturbing signals, but in the next rows, the required noise for bringing the MFR down, has grown progressively. This effect must be relative to the area of the fixed point's attraction basin, when escaping the limit cycle. Pinpointing the structure of the attraction borders is more challenging, in this setting; because depending on the time point (phase state of the SLC) when the phase trajectories leave the SLC, the probability of ending up in the rest state varies. As mentioned before, this is due to the non-autonomous nature of this neural system which is under our discussion.

However, the evolution of these time-relevant changes in the basin structure is continuous and can be understood by looking at several snap-shots at key time points along the limit cycle. Since the comprising neurons are identical, and the SLC is symmetric, we can confine our time-point to half of its period. To obtain these snap-shots, we prepare the network in the following manner: The persistent activity is switched on in the network and transients are integrated out over 200 ms. Then eight time spots, uniformly distributed on half of the limit cycle, are chosen and the methods as above are applied to find the attraction domains at those specific moments. Results are shown in Fig. 11 for four parameter points moving upward in the parameter space on the vertical line; $I_{ext} = -1$, with different synaptic strengths coming from the set J $\in$ {5.8, 6, 7, 11}. In this figure, the dark black squares on each SLC's path, indicate the time point for which the attraction basins are found.

It is clear that close to the network bifurcation, almost all of the phase plane is most often covered by the attraction domain of the rest state. From bottom upward the parameter space, the purple regions of the phase planes, corresponding to the attraction basin of rest states are shrinking. Consequently, close to the global bifurcation border, it is highly probable that even weak noise can force a phase trajectory to escape the limit cycle and land it somewhere in the vast purple regions of silence. But far from the bifurcation, the phase planes are vastly, and most often covered by the SLC's attraction basin, and thus noise is less likely to switch the activity off. That is why the falling slope of the ISR curves are steep close to the global bifurcation, but getting farther from this border, decreases the probability of switch off, and results in a mild MFR descent.

4. Conclusions

In summary, we showed that independent noise can induce Inverse Stochastic Resonance in a minimal network of two type I excitable neurons where a bistability between the rest and a synaptically induced limit cycle exists. Independent noises of tuned variance can switch the network from the persistent stable limit cycle (SLC) to the rest in a finite short time

(e.g. after 1 or two spikes). At this noise level the return to the SLC from the rest is not observed even in long simulations (similar to what was show in [47]). Noise above this optimal variance induces intermittent SLC bursts. Hence the ISR curve appears. We also show that ISR characteristics depend on the parameters of the network, notably on how far is the network from the bifurcations: 1. Above the bifurcation for the onset of the synaptically induced bistability and 2. Below the saddle-node bifurcations for the individual neurons – where they become intrinsic oscillators. ISR is most apparent farther below the second bifurcation. We further showed that computing the mutual information between a periodic input to the network and its output, we observe stochastic resonance: a tuned noise level with maximal MI. Importantly, the SR curves coincide with the ISR tuning – hence ISR implies SR. in other words, ISR ensures optimal transfer of information through the network.

We might speculate that levels of intrinsic noise maybe dynamically regulated in brain circuits to toggle these networks from persistent activity attractor domain (active memory encoding) and feed-forward information transfer modes. How might the ISR and SR appear in larger and/or more biologically realistic networks of excitatory and inhibitory neurons, how these depend on the noise correlations and synaptically introduced noise remain a subject for future investigation.

Acknowledgments

This study was supported by Russian Science Foundation grant (No: 17-11-01273).

Supplementary materials

Supplementary material associated with this article can be found, in the online version, at doi:10.1016/j.cnsns.2019.105024.

References

[1] Miller EK, Erickson CA, Desimone R. Neural mechanisms of visual working memory in prefrontal cortex of the macaque. J Neurosci 1996;16(16):5154–67.
[2] Goldman-Rakic P. Cellular basis of working memory review. Neuron 1995;14:477–85.
[3] Fransén E, Alonso AA, Hasselmo ME. Simulations of the role of the muscarinic-activated calcium-sensitive nonspecific cation current in entorhinal neuronal activity during delayed matching tasks. J Neurosci 2002;22(Feb (3)):1081–97.
[4] Egorov AV, Hamam BN, Fransén E, Hasselmo ME, Alonso AA. Graded persistent activity in entorhinal cortex neurons. Nature Nov. 2002;420:173.
[5] Suzuki WA, Miller EK, Desimone R, Wendy A, Miller EK, Ob RD. Object and place memory in the Macaque Entorhinal Cortex. J Neurophysiol 1997;78(2):1062–81.
[6] Axmacher N, Mormann F, Fernández G, Cohen MX, Elger CE, Fell J. Sustained neural activity patterns during working memory in the human medial temporal lobe. J Neurosci 2007;27(Jul (29)):7807–16.
[7] Young BJ, Otto T, Fox GD, Eichenbaum H. Memory representation within the parahippocampal region. J Neurosci 1997;17(Jul (13)):5183–95.
[8] Schon K, Hasselmo ME, LoPresti ML, Tricarico MD, Stern CE. Persistence of parahippocampal representation in the absence of stimulus input enhances long-term encoding: a functional magnetic resonance imaging study of subsequent memory after a delayed match-to-sample task. J Neurosci 2004;24(Dec (49)):11088–97.
[9] Hollerman JR. Changes in behavior-related neuronal activity in the striatum during learning. Trends Neurosci 2003;26(6):321–8.
[10] Komura Y, Tamura R, Uwano T, Nishijo H, Kaga K, Ono T. Retrospective and prospective coding for predicted reward in the sensory thalamus. Nature Aug. 2001;412:546.
[11] Kojima J, Matsumura M, Togawa M, Hikosaka O. Tonic activity during visuo-oculomotor behavior in the monkey superior colliculus. Neurosci Res 1996;26:17–28.
[12] Moschovakis AK. The neural integrators of the mammalian saccadic system. Front Biosci 1997;2:552–77.
[13] Prut Y, Fetz EE. Primate spinal interneurons show pre-movement instructed delay activity. Nature Oct. 1999;401:590.
[14] Major G, Tank D. Persistent neural activity : prevalence and mechanisms. Curr Opin Neurobiol 2004;14(6):675–84.
[15] Amit DJ, Brunel N. Model of global spontaneous activity and local structured activity during delay periods in the cerebral cortex. Cereb Cortex 1997;7(3):237–52.
[16] Novikov N, Gutkin B. Robustness of persistent spiking to partial synchronization in a minimal model of synaptically driven self-sustained activity. Phys Rev E 2016;94(Nov (5)):52313.
[17] Faisal AA, Selen LPJ, Wolpert DM. Noise in the nervous system. Nat Rev Neurosci 2008;9(April):292–303.
[18] McDonnell MD, Ward LM. The benefits of noise in neural systems: bridging theory and experiment. Nat Rev Neurosci 2011;12(7):415–26.
[19] Gutkin T, Boris S, Jost J, Henry C. Inhibition of rhythmic neural spiking by noise: the occurrence of a minimum in activity with increasing noise. Naturwissenschaften 2009;96:1091–7.
[20] Wiesenfeld K, Moss F. Stochastic resonance and the benefits of noise: from ice ages to crayfish and SQUIDs. Nature 1995;373(6509):33–6.
[21] Benzi R, Sutera A, Vulpiani A. The mechanism of stochastic resonance. J Phys A Math Gen 1981;14(Nov (11)):L453–7.
[22] McNamara B, Wiesenfeld K. Theory of stochastic resonance. Phys Rev A 1989;39(9):4854–69.
[23] Gammaitoni L, Martinelli M, Pardi L, Santucci S. Observation of stochastic resonance in bistable electron-paramagnetic- resonance systems. Phys Rev Lett 1991;67(13):1799–802.
[24] Douglass JK, Wilkens L, Pantazelou E, Moss F. Noise enhancement of information-transfer in crayfish mechanoreceptors by stochastic resonance. Nature 1993;365(6444):337–40.
[25] Russell DF, Wilkens LA, Moss F. Use of behavioural stochastic resonance by paddle fish for feeding. Nature 1999;402(6759):291–4.
[26] Schmid G, Goychuk I, Hänggi P. Stochastic resonance as a collective property of ion channel assemblies. Europhys Lett 2001;56(1):22–8.
[27] Longtin A. Stochastic resonance in neuron models. J Stat Phys 1993;70(1):309–27.
[28] Moss F, Ward LM, Sannita WG. Stochastic resonance and sensory information processing: a tutorial and review of application. Clin Neurophysiol 2004;115(2):267–81.
[29] Kawaguchi M, Member S, Mino H, Member S, Durand DM. Stochastic resonance can enhance information transmission in neural networks. IEEE Trans Biomed Eng 2011;58(7):1950–8.
[30] Mitaim S, Kosko B. Adaptive stochastic resonance in noisy neurons based on mutual information. IEEE Trans Neural Networks Nov. 2004;15(6):1526–40.
[31] Gutkin B, Hely T, Jost J. Noise delays onset of sustained fring in a minimal model of persistent activity. Neurocomputing 2004;60:753–60.
[32] Tuckwell HC, Jost J, Gutkin BS. Inhibition and modulation of rhythmic neuronal spiking by noise. Phys Rev E - Stat Nonlinear, Soft Matter Phys 2009;80(3).
[33] Gutkin BS, Jost J, Tuckwell HC. Transient terminationof spiking by noise in coupled neurons. Europhys Lett 2007;81(Dec (2)):20005.

[34] Gutkin B, Jost J, Tuckwell HC. Random perturbations of spiking activity in a pair of coupled neurons. Theory Biosci 2008;127(May (2)):135–9.
[35] Tuckwell HC, Jost J. Weak noise in neurons may powerfully inhibit the generation of repetitive spiking but not its propagation. PLoS Comput Biol 2010;6:e1000794.
[36] Tuckwell HC, Jost J. The effects of various spatial distributions of weak noise on rhythmic spiking. J Comput Neurosci 2011;30:361–71.
[37] Uzuntarla M, Cressman JR, Ozer M, Barreto E. Dynamical structure underlying inverse stochastic resonance and its implications. Phys Rev E Stat Nonlin Soft Matter Phys 2013;88(4):42712.
[38] Paydarfar D, Forger DB, Clay JR. Noisy inputs and the induction of on-off switching behavior in a neuronal pacemaker. J Neurophysiol 2006;96 6:3338–48.
[39] Buchin A, Rieubland S, Häusser M, Gutkin BS, Roth A. Inverse stochastic resonance in cerebellar Purkinje cells. PLoS Comput Biol 2016;12:e1005000.
[40] Guo D. Inhibition of rhythmic spiking by colored noise in neural systems. Cogn Neurodyn 2011;5(3):293–300.
[41] Ermentrout B. Type I membranes, phase resetting curves, and synchrony. Neural Comput 1996;8:979–1001.
[42] Pocock A. "MIToobox for C and Matlab." [Online]. Available: http://www.cs.man.ac.uk/~pococka4/MIToolbox.html.
[43] Borst A, Theunissen FE. Information theory and neural coding. Nat Neurosci 1999;2:947–57.
[44] Manwani A, Koch C. Detecting and estimating signals over noisy and unreliable synapses: information-theoretic analysis. Neural Comput 2001;13:1–33.
[45] Brown G, Pocock A, Zhao M-J, Luján M. Conditional likelihood maximisation : a unifying framework for information theoretic feature selection. J Mach Learn Res 2012;13:27–66.
[46] Uzuntarla M. Inverse stochastic resonance induced by synaptic background activity with unreliable synapses. Phys Lett A 2013;377(38):2585–9.
[47] Tuckwell HC, Jost J. Analysis of inverse stochastic resonance and the long-term firing of Hodgkin–Huxley neurons with Gaussian white noise. Phys A Stat Mech its Appl 2012;391(22):5311–25.
[48] Uzuntarla M, Barreto E, Torres JJ. Inverse stochastic resonance in networks of spiking neurons. PLOS Comput Biol 2017;13(7):1–23.